METASTABLE AMORPHOUS PHASE OF TELLURIUM-BASE ALLOYS

Thesis by

Huey-Lin Luo

In Partial Fulfillment of the Requirements

For the Degree of

Doctor of Philosophy

California Institute of Technology

Pasadena, California

1964

ACKNOWLEDGEMENT

The writer of this thesis wishes to express his appreciation to Professor P. Duwez for his direction and encouragement. He also wishes to thank Professor F. S. Buffington for his careful reading of the manuscript and many helpful suggestions, and Professor C. J. Pings for his valuable discussions and his help in connection with the computer programming. Acknowledgement is due to the U. S. Atomic Energy Commission through whose financial support this investigation has been made possible.

ABSTRACT

Amorphous phases have been found in tellurium base alloys very rapidly cooled from the liquid state. These phases, which are stable at room temperature, exist in binary alloys containing from approximately 10 to 25 at. % germanium, and from 10 to 30 at. % of gallium or indium. The structure of these alloys was studied by x-ray diffraction (Debye-Scherrer method), using molybdenum Kα radiation monochromatized by the (200) plane of a lithium fluoride crystal. Radial distribution functions were obtained for several alloys and within the experimental accuracy neither the nature of the alloying element nor its concentration had a noticeable effect on the shape of the distribution function. The atomic arrangement in the amorphous alloys is very similar to that found in liquid tellurium which is itself closely related to the crystal structure of solid tellurium. The existence of amorphous phases in tellurium base alloys is discussed in relation with previously published ideas on the various factors governing glass formation in solids.

TABLE OF CONTENTS

TABLE OF FIGURES

I. INTRODUCTION AND LITERATURE REVIEW

The study of x-ray diffraction by liquids started when Debye and Scherrer became aware of the diffraction haloes produced by liquid benzene (1). More definite evidence was shown by Keesom and de Smedt who confirmed the existence of diffraction haloes from liquid argon, oxygen and nitrogen (2). Thereafter, x-ray studies of liquids were carried out by many workers. Review articles by Gingrich (3), Furukawa (4) and Kruh (5) provided a rich collection of data and references in this field.

The modern theoretical basis of diffraction by liquids was established by Zernike and Prins who applied the Fourier integral theorem to calculate a probability function (the radial distribution function) of molecules around an individual molecule from the observed diffraction intensity (6). Debye and Menke first used this method to obtain quantitative information in the study of liquid mercury (7). Since then, many advances have been made in the liquid structure studies and the development of electronic computers made it possible to carry out extensive calculations. However, in the process of experiments and the calculation of radial distribution functions, some systematic errors were involved. Finbak examined such errors closely and suggested corresponding corrections (8-10). Thus, often the experimental data on x-ray intensity require careful analysis in order to reach correct physical interpretation.

Amorphous solids including glasses are quite different from liquid in physical and mechanical properties but show remarkable

resemblance in x-ray diffraction patterns. Thus the analytical method used in studying liquids is applicable to amorphous solids as well. Aside from numerous glasses for which systematic survey by x-ray analysis has been conducted, the work on amorphous materials has been mostly concentrated on pure elements. Thus amorphous state of all these elements except sulfur and selenium could only be obtained in the form of thin films by vacuum deposition. Nearly all the x-ray work on amorphous and glassy systems has been reviewed by Warren (11), Richter (12), Richter and Steeb (13) and Urnes (14); the "Bibliography on Glass Structure" (15) compiled by the American Ceramic Society also provides information on early work of glasses.

The existence of elementary selenium in the amorphous form has been reported by several authors. Besides vacuum deposition, amorphous selenium was obtained by rapidly cooling molten selenium (16, 17), by precipitation through chemical processes (17-19), and by chilling hot selenium powder with air stream (20). Richter and coworkers (19, 21-23) made thorough investigations by x-ray diffraction of amorphous and liquid selenium and found practically the same pattern. They tried to interpret their results as indicating the presence of ring and chain structure in some region. Because tellurium is isomorphic with selenium, some authors simply claimed that it was possible to undercool tellurium into an amorphous state (24-26). However, no real evidence could be found to substantiate this statement.

This thesis is concerned with the study of amorphous phases in tellurium-base alloys obtained by a recently developed technique of

rapid cooling. Since only small amounts of alloys can be obtained in each quenching experiment, only x-ray diffraction experiments were conducted. The calculation of the radial distribution functions was carried out with proper corrections and an attempt is made to correlate the results with the structure of liquid tellurium (27).

II. ALLOY PREPARATION AND QUENCHING TECHNIQUES

In the present investigation, metastable amorphous phases were obtained in binary tellurium-base alloys with 10 ~ 30 at. % Ga, 10 ~ 25 at. % Ge, and 10 ~ 30 at. % In. Alloys were prepared in 2 to 4 gm lots from elements of purity greater than 99. 9%. Weighed quantities were first melted under hydrogen in quartz or alumina crucibles which were in contact with an induction heated graphite block. After reweighing, the alloys were cast into 1 mm wires under argon. Typical weight losses for all tellurium-rich alloys were less than 0. 2%.

Short lengths (about 30 mg) of the alloy wires were heated to 600 ~ 700 ^{o}C in either graphite nozzles or alumina inserts in graphite nozzles which were in turn heated by induction heating. The molten alloy was then shot by a blast of helium onto polished copper or lightly sandblasted aluminum strips held on the inner periphery of a rotating wheel. Liquid alloy charges were thus solidified into well-spread flakes and were ready to be removed from substrates. Details of this quenching technique have been described previously (28, 29).

III. X-RAY DIFFRACTION PROCEDURES AND RESULTS

For x-ray diffraction work, 114.6 mm diameter Debye-Scherrer cameras were used with molybdenum K-radiation monochromatized by the 200-plane of a lithium fluoride single crystal. Typical exposures were for 150 hours at 45 kv and 18 ma, using the Ansco Superay-C film.

A roughly rectangular flake of 2 mm x 0.3 mm in dimension was cut from the quenching alloy sample, stuck onto a quartz fiber with celvacene and positioned normal to the incident beam with the long edge across the film. Care was taken to keep the tip of the glass fiber outside the beam. X-ray exposure was made with the specimen stationary. The thicknesses of quenched alloy samples were measured by the absorption of a normally incident monochromatized x-ray beam. For the systems Ga-Te, Ge-Te, and In-Te at different compositions, the result of measurements shows thicknesses ranging from 4 to 10 microns.

In addition to the flake samples, powder specimens were made by grinding the quenched alloys in a boron carbide mortar to 200 mesh or less and packing into thin-walled glass capillaries of 0.5 mm diameter. Exposed films were developed according to a unique standard procedure recommended by the film manufacturer.

The intensity of an x-ray beam diffracted by a specimen may be measured by the amount of blackening it produces on a photographic film. The photographic density D, or blackening, of a film may in turn be measured by the amount of visible light transmitted through the film. For each type of x-ray film there is a specific relationship between the density and the exposure which is defined as the intensity of x-ray beam

multiplied by time. Since the time is constant for the entire portion of each film, the exposure is directly proportional to the x-ray intensity.

For the Ansco Superay-C films used in this investigation, the characteristic curve supplied by the manufacturer is accurate within 10%. The portion of this curve that is effective in the present study may be reasonably taken as linear if the 10% error is considered. Thus throughout this investigation, a linearly proportional relation between the film density and the x-ray intensity is assumed.

The film density was measured by means of an ARL microphotometer. Typical microphotometric traces for a rotational specimen are shown in Fig. 1 and 2. For the purpose of comparison, traces of stationary specimens for alloys of the same composition are also shown. The apparent disagreement between these two traces is due probably to distinct absorption effects induced by the difference in geometry of the two types of specimens. Since the geometry of stationary specimens is not definite, only the results from rotational specimens were studied further.

The film density D, as a function of the glancing angle θ, is obtained from the microphotometer reading S by the formula (30)

$$D(\theta) = - \log S + \log S_o$$

where S_o is the reading for a strip of unexposed but regularly developed film. The directly observed intensity data cannot be taken as the real diffraction pattern of the specimen until they have been properly corrected for polarization and absorption. In addition, in view of certain systematic errors, Finbak has suggested a further correction which is to

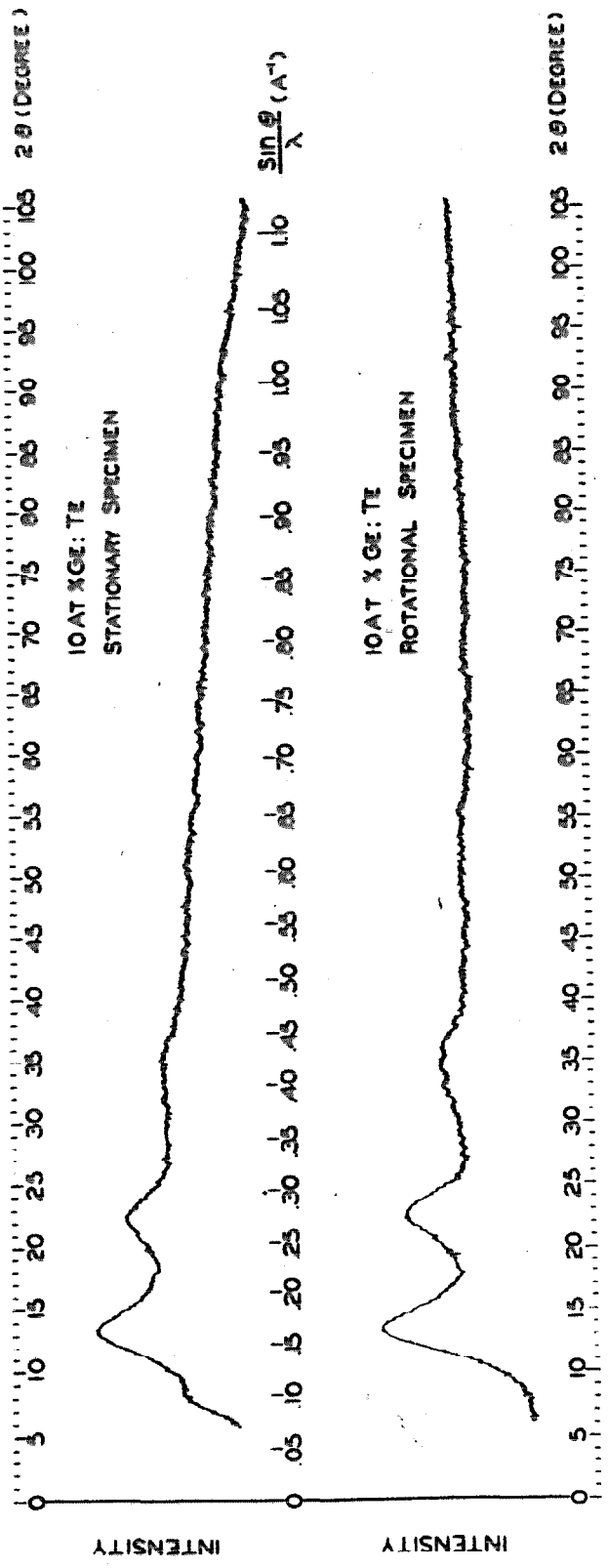

Fig. 1. Microphotometric traces of x-ray diffraction patterns for the alloy 10 at. % Ge:Te.

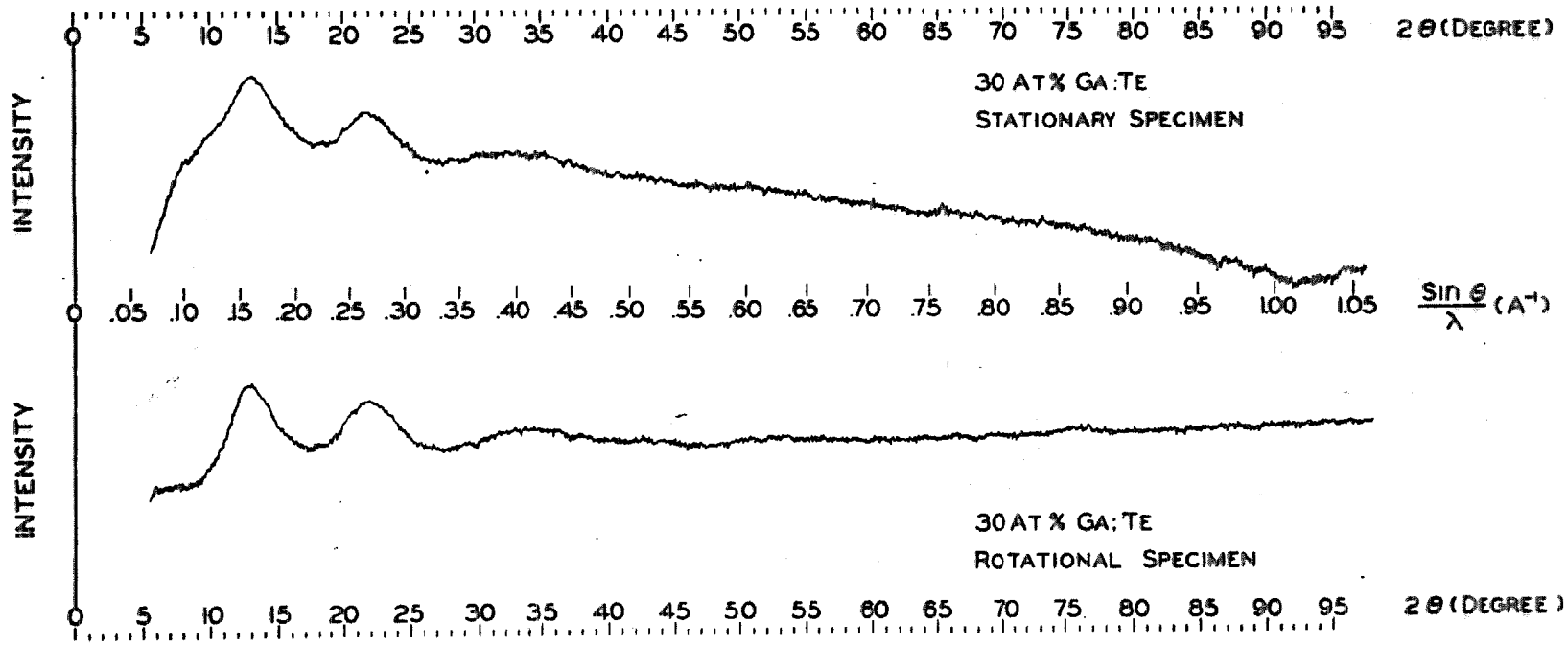

Fig. 2. Microphotometric traces of x-ray diffraction patterns for the alloy 30 at. % Ga;Te.

be carried out with the normalization procedure (Finbak correction) (8).

Unpolarized radiation from the x-ray target undergoes partial polarization when reflected from the crystal monochromator and also when scattered by the amorphous sample. It can be shown that in referring to the unpolarized level the observed intensity is to be divided by the factor (31)

$$P(\theta) = \frac{1 + \cos^2 2\theta' \cos^2 2\theta}{1 + \cos^2 2\theta'}$$

in which θ' is the Bragg angle for the reflecting planes of the monochromatizing crystal. Thus for the (200) plane of lithium fluoride ($d = 2.0135$ Å) and molybdenum K_α radiation ($\lambda = 0.71069$ Å), $\theta' = 10^\circ 9.9'$.

In all diffraction techniques the incident and diffracted beams in passing through the irradiated specimen are partially absorbed, so that the diffracted beams are less intense than they would be if the specimen were completely nonabsorbing. The nature of the absorption correction depends upon the experimental arrangement, or the geometry of the specimen. The correction for absorption in a cylindrical specimen is so complicated that it has been often neglected. Claassen (32), assuming an essentially parallel incident beam of x-rays which completely bathed the specimen, gave the ratio of the intensity of the diffracted beam to that of the same beam without absorption as

$$A(\theta) = \frac{1}{\pi r^2} \int\int e^{-\mu l} d\sigma$$

where r is the radius of the specimen, μ the linear absorption coef-

ficient of the specimen, l the total path length of the ray in the specimen before and after being scattered by a small volume fragment and $d\sigma$ a small element of cross section. Rusterholz showed that for fairly highly absorbing substances the absorption factor was a rather simple function of the glancing angle (33). By combining both, Bradley arrived at a workable method to calculate the absorption factor for cylindrical powder samples in general (34). Bradley's treatment is essentially dividing the entire cross section into three portions and approximating separately the above integral expression by finite series. The total absorption effect is simply the sum of the contributions from these three areas. Thus the experimental intensity data are to be divided by the expression

$$A(\theta) = \sum_{n=1}^{7} \frac{a_n n!}{\mu^n r^n}$$

with a_n given as function of θ.

$$A = \frac{a_1}{\mu r} + \frac{a_2}{(\mu r)^2} + \frac{a_3}{(\mu r)^3} + \frac{a_5}{(\mu r)^5} + \frac{a_7}{(\mu r)^7}$$

$$a_1 = \frac{1}{\pi}\left[1 - \frac{\log(\sec\theta + \tan\theta)}{\sec\theta \tan\theta}\right]$$

$$a_2 = \frac{1}{2\pi} \sin 2\theta$$

$$a_3 = \frac{3!}{\pi}\left(-\frac{1}{3}\frac{1}{2^3} + \frac{1}{2^3}x\right)$$

$$a_5 = \frac{5!}{\pi}\left[-\frac{1}{5}\frac{1}{27} + \frac{1}{27}\cos^2\theta\left(\frac{1}{4} + \frac{3}{4}x\right)\right]$$

$$a_7 = \frac{7!}{\pi}\left\{-\frac{1}{2^{10}}\frac{1}{7} + \frac{1}{2^{10}}\cos^2\theta\left[\frac{1}{6} + \frac{5}{6}\cos^2\theta\left(\frac{1}{4} + \frac{3}{4}x\right)\right]\right\}$$

where

$$x = \cos^2\theta \left[\frac{1}{2} + \frac{1}{2} \frac{\log (\sec \theta + \tan \theta)}{\sec \theta \tan \theta} \right].$$

Thus the experimental intensity is obtained as

$$I_e(\theta) \sim \frac{D(\theta)}{P(\theta)A(\theta)}$$

For the convenience of calculation, these quantities are usually expressed in terms of $s = \frac{4\pi \sin \theta}{\lambda}$ where λ is the wavelength of the monochromatized x-ray beam.

In the course of x-ray scattering, the process of incoherent scattering always occurs. Since this type of scattering plays no part in interferences but introduces a slowly varying background, its effect must be subtracted from the experimental data. The intensity of the incoherent scattering is given in electron units as a function of $v = 0.176\, s/Z^{2/3}$ by

$$I_{inc.} = BZH(v) .$$

In this expression, Z is the atomic number; H is derived by Heisenberg (35) and given numerically by Bewilogua for $Z > 6$ (36). B is the relativistic Breit-Dirac factor defined as (37)

$$B = \left[1 + \frac{2h\lambda}{mc} \left(\frac{\sin \theta}{\lambda} \right)^2 \right]^{-3}$$

with h being the Planck's constant, c the speed of light, and m the electron mass.

Experimentally, it is difficult to measure the scattered intensity

below a certain value of s because the main x-ray beam is present. To correct for the inaccessibility of this small angle scattering, it is convenient to subtract out the intensity at small angles, $I_o(s)$, by using the facts that (38)

$$\lim_{s \to 0} \left[I(s) - I_o(s) \right] = 0$$

and that $I_o(s)$ differs significantly from zero only near $s = 0$. Practically, this is done by simply extrapolating the measured $I(s)$ vs. s curve to zero at $s = 0$ (4).

After making the above corrections, the experimental intensity is still in an arbitrary unit. In practice, these data must be expressed in units of classical electron scattering in order to make quantitative interpretation. Generally, this is done by assuming that at large glancing angles where interference effects can be neglected, the observed coherently scattered x-rays have the same intensity as that produced by the same number of atoms which scatter x-rays independently. Thus the method consists of evaluating a scaling factor, a_1, to bring the observed intensity close to the independent atomic scattering at high angles, i.e.,

$$a_1 = \lim_{s \text{ large}} \left[\frac{N(f^2 + I_{inc})}{I_e - I_o} \right]$$

where N is the number of atoms per unit volume and f is the atomic scattering factor.

A second criterion for normalization proposed by Krogh-Moe was based on integrated intensities (39). This criterion supplies another

scaling constant given as

$$a_2 = \frac{N\int_0^\infty s^2(f^2 + I_{inc})\,ds - 2\pi^2 NZ\bar{\rho}}{\int_0^\infty s^2(I_e - I_o)\,ds}$$

where $\bar{\rho}$ is the average electronic density. It can be seen immediately that this criterion differs from the first one by taking into consideration the whole range of intensity data instead of accounting for the intensities at high-angle only.

Thus the experimental intensity is normalized to

$$I_e(s) = a\frac{D(s)}{P(s)A(s)}$$

with a given by either one of the criteria. The data then are used for the calculation of the distribution function.

However, after careful study and comparison step by step, Finbak (8) concluded that there might still be an uncontrolled systematic error involved in the intensity data thus handled. The characteristic of this type of error is that it equals zero for small s, reached its greatest value for $s = 1 \sim 2$ Å^{-1} where the intensity curve generally has its highest peak, and decreases uniformly to zero with increasing s. In other words, this wedge-shaped error exaggerates the first peak of the intensity data. Consequently a maximum is introduced in the distribution function at 0.3 ~ 1.0 Å. Physically, the distribution function can not have any maximum in this region. In the present investigation, it has been found that this is indeed the case. To correct this type of error, Finbak introduced an additive term in the normalization process,

namely,

$$I_e(s) = \frac{aD(s)+b}{P(s)A(s)}$$

and stated that the constants a and b were to be determined by a trial and error method. However, with two criteria for normalization at hand, it seems logical to use both of them to determine the two constants simultaneously. Fig. 3 shows a comparison of the intensity with and without this additive term correction for the alloy 10 at.% Ga;Te. The corrected intensity data for alloys 25 at.% Ga;Te, 25 at.% Ge;Te and 25 at.% In;Te are shown subsequently in Figs. 4, 5, and 6.

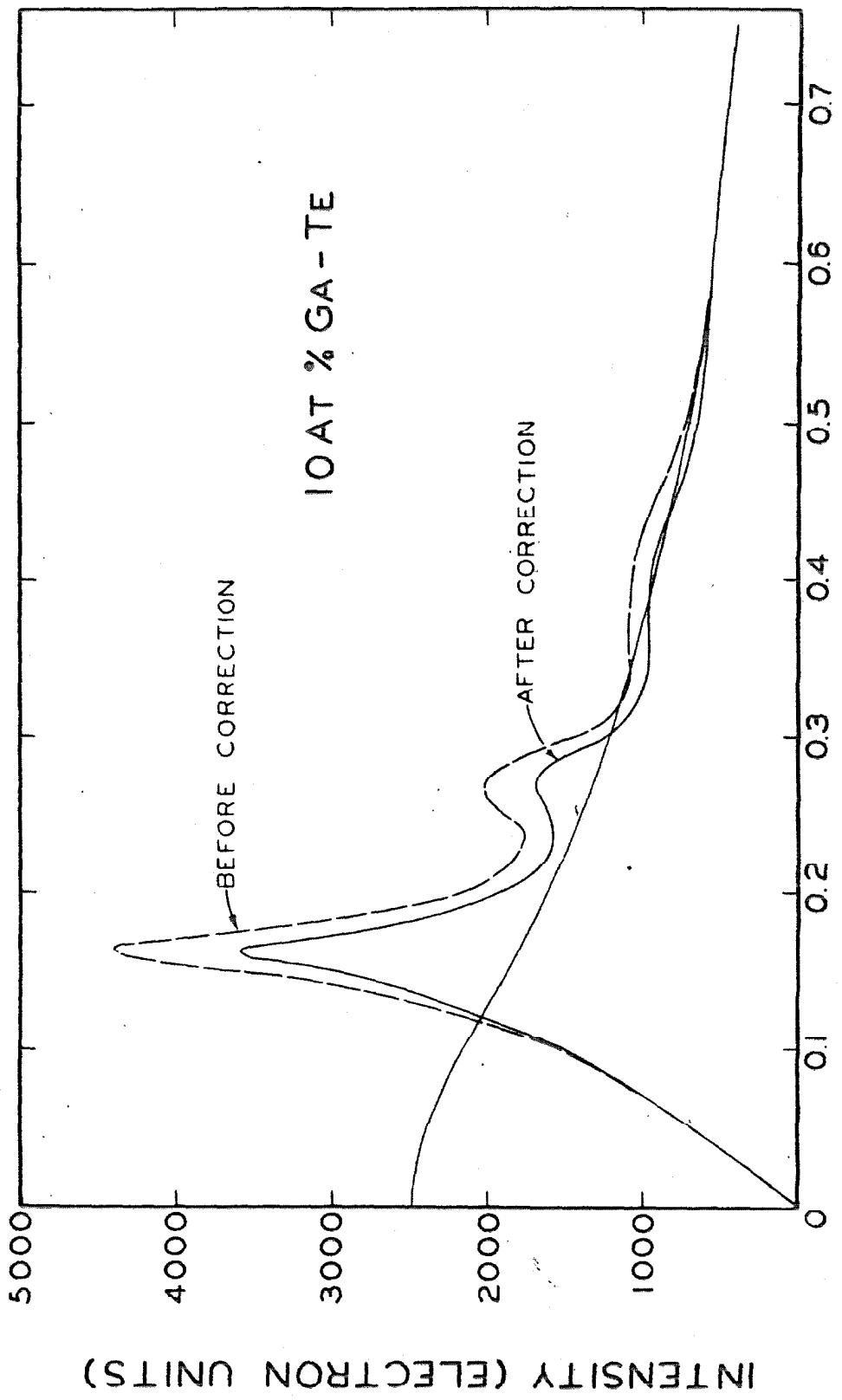

Fig. 3. Intensity curves for 10 at. % Ga; Te before and after normalization correction.

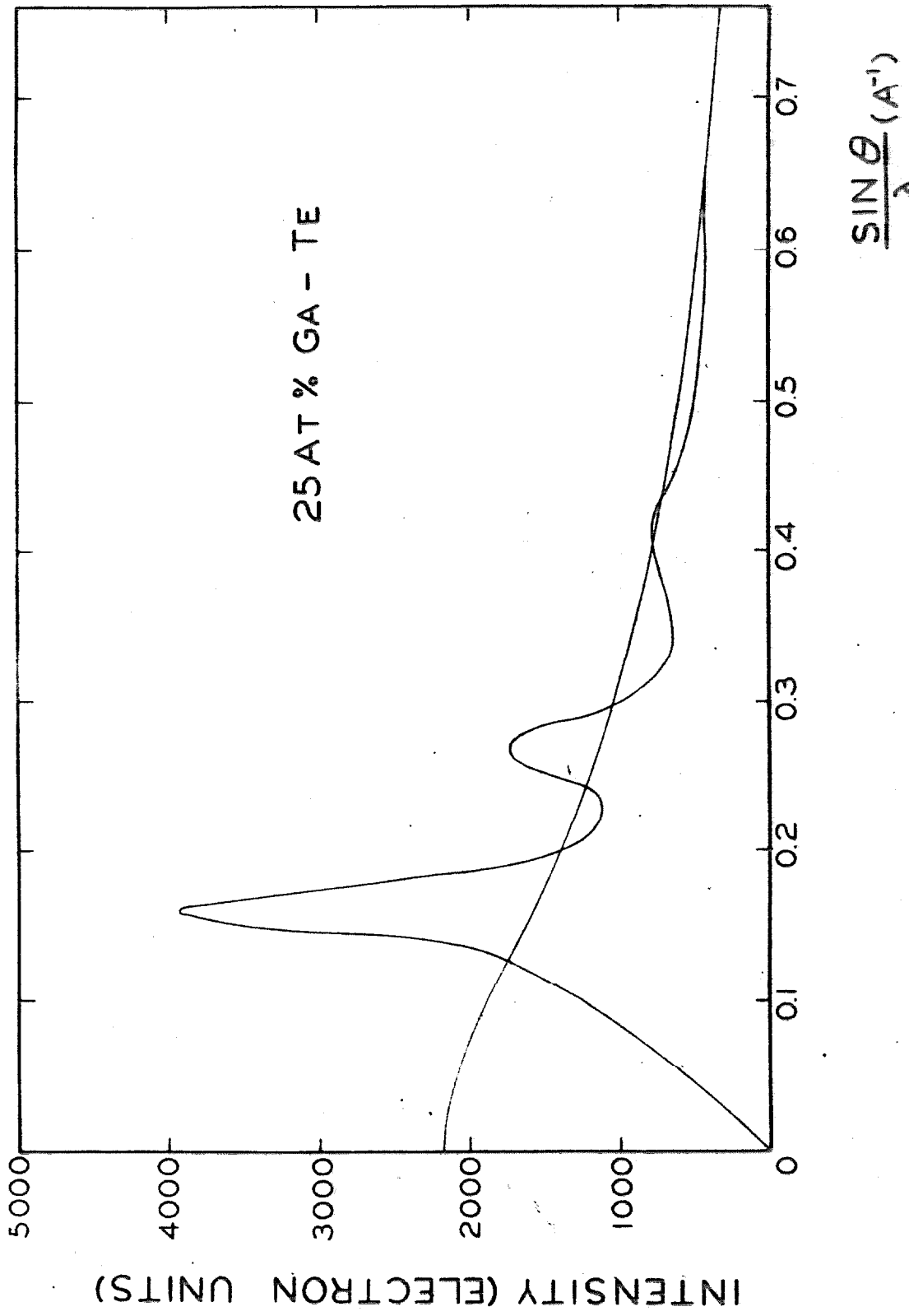

Fig. 4. Corrected intensity curve for 25 at. % Ga; Te.

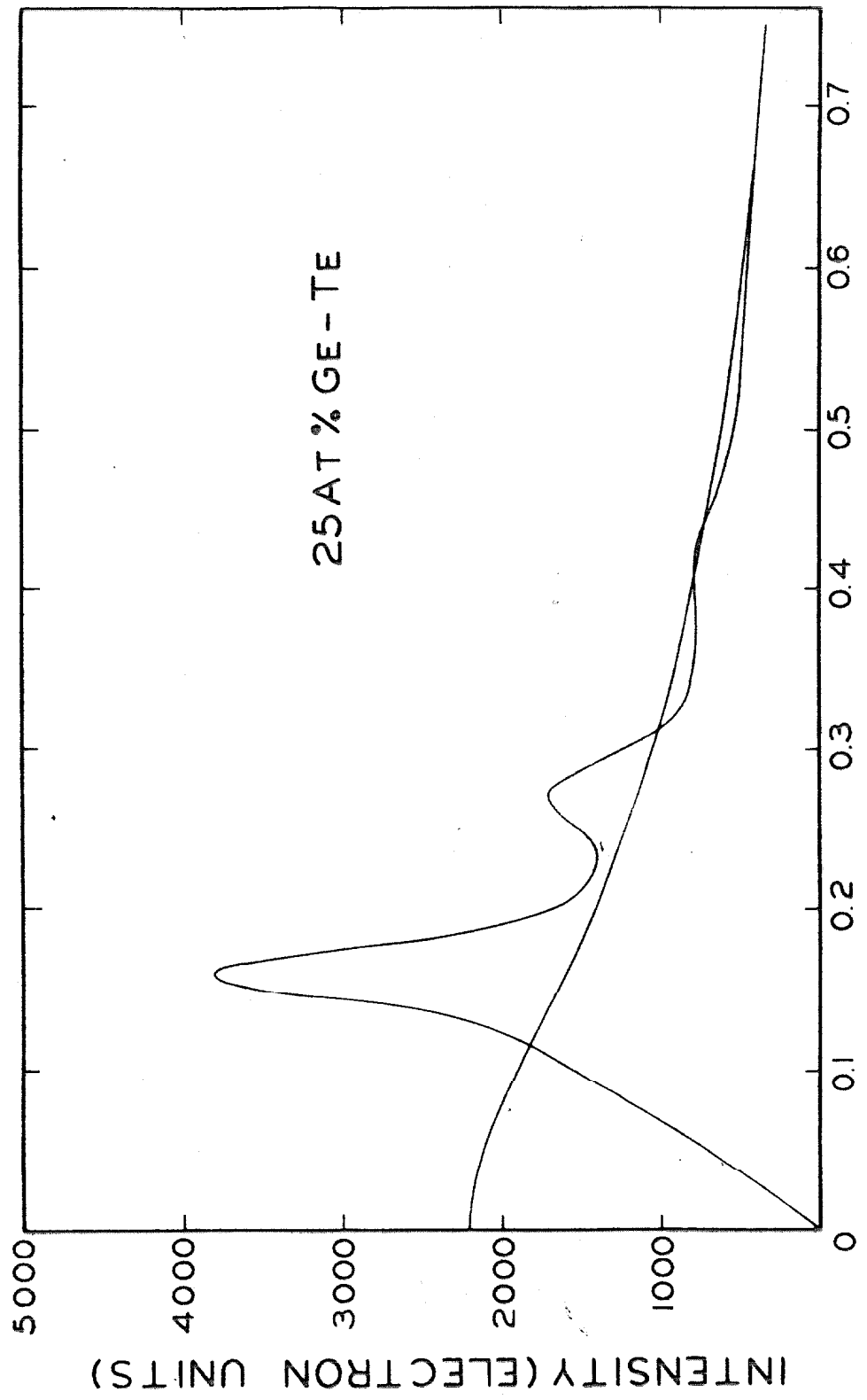

Fig. 5. Corrected intensity curve for 25 at. % Ge;Te.

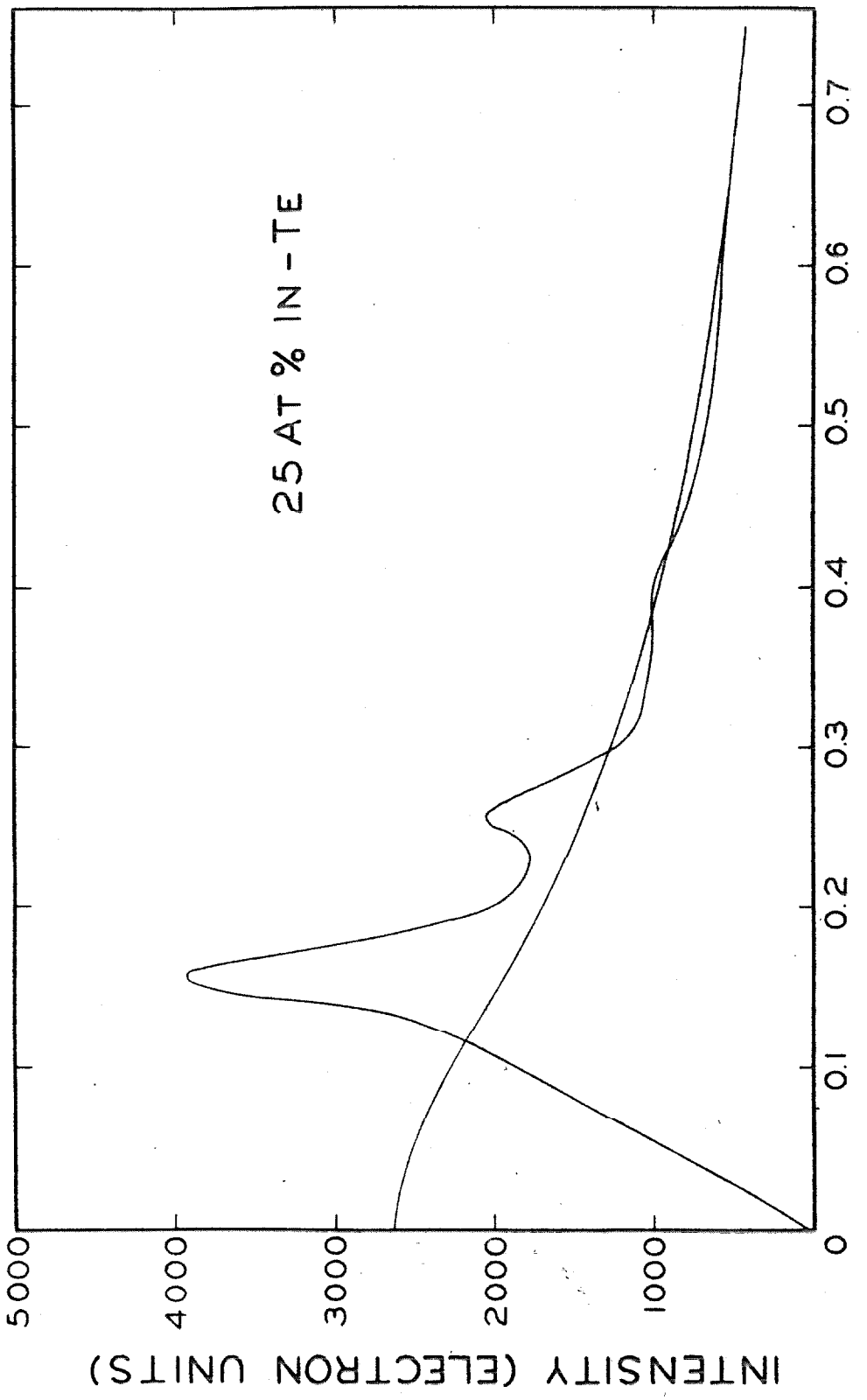

Fig. 6. Corrected intensity curve for 25 at. % In;Te.

IV. CALCULATION OF RADIAL DISTRIBUTION FUNCTIONS

The intensity in electron units scattered by a non-crystalline array of atoms at an angle θ is given by Debye's equation (40)

$$I(s) = \sum_{n,m} f_n f_m \frac{\sin sr_{nm}}{sr_{nm}}$$

where f_n, f_m are the atomic scattering factors for the n^{th} and m^{th} atoms respectively; r_{nm} is the distance separating these two atoms.

In the present investigation, since the amorphous structure is observed over a range of compositions for different systems, it is assumed that the two kinds of atoms in each alloy occupy random positions in the amorphous structure. An average scattering factor and atomic number are then introduced in the computations. In other words, it is considered that in an amorphous phase consisting of two elements, the atoms are distributed at random so that the phase is regarded as being made of one kind of average atoms. Hence

$$f_m = f_n = f, \qquad f_n f_m = f^2 .$$

In performing the summation, it is necessary to consider one atom as origin and to carry out the summation over all distances to all atoms of the specimen, including the one at the origin, and then to allow every atom of the specimen to become the origin atom. Summations for any atom with respect to itself lead to unity. Thus for N atoms in all,

$$I(s) = Nf^2(s)\left[1 + \sum_{n} \frac{\sin sr_{nm}}{sr_{nm}}\right]$$

where the summation excludes the origin atom.

Furthermore, it is assumed that in noncrystalline phases the distribution of atoms is continuous; then the above summation may be replaced by an integral, i.e.,

$$I(s) = Nf^2(s) \left[1 + \int_0^R 4\pi r^2 \rho(r) \frac{\sin sr}{sr} \, dr \right].$$

In this expression, $\rho(r)$ is the density of atoms at distance r from the origin atom, hence $4\pi r^2 \rho(r)\, dr$ is the number of atoms in a spherical shell of radius r and thickness dr; and R is a measure of dimension of the noncrystalline specimen which is very large compared with the microscopic value r. Rewrite the above equation by introducing ρ_o as the constant average density of atoms.

$$I(s) = Nf^2 \left[1 + \int_0^R 4\pi r^2 \left(\rho(r) - \rho_o \right) \frac{\sin sr}{sr} \, dr + \int_0^R 4\pi r^2 \rho_o \frac{\sin sr}{sr} \, dr \right].$$

The second integral corresponds to the small-angle scattering intensity of uniformly dense material which is usually unobservable because of the presence of the main beam. Hence, if attention is limited to experimentally observable intensities, this integral can be taken as zero (41). It can be expected that within a noncrystalline system $\rho(r)$ rapidly approaches ρ_o when r becomes several atomic diameters; thus R is safely taken as infinity. Then

$$si(s) = \int_0^\infty 4\pi r \left[\rho(r) - \rho_o \right] \sin sr \, dr$$

where

$$i(s) = \frac{I(s)}{Nf^2(s)} - 1 \ .$$

By Fourier integral theorem, the above equation is transformed into

$$r\left[\rho(r) - \rho_o\right] = \frac{1}{2\pi^2}\int_o^\infty si(s) \sin rs \, ds$$

or

$$4\pi r^2\rho(r) = 4\pi r^2\rho_o + \frac{2r}{\pi}\int_o^\infty si(s) \sin rs \, ds \ .$$

With the help of an electronic computer, the data shown in Figs. 3-6 are calculated and plotted in Figs. 7-10.

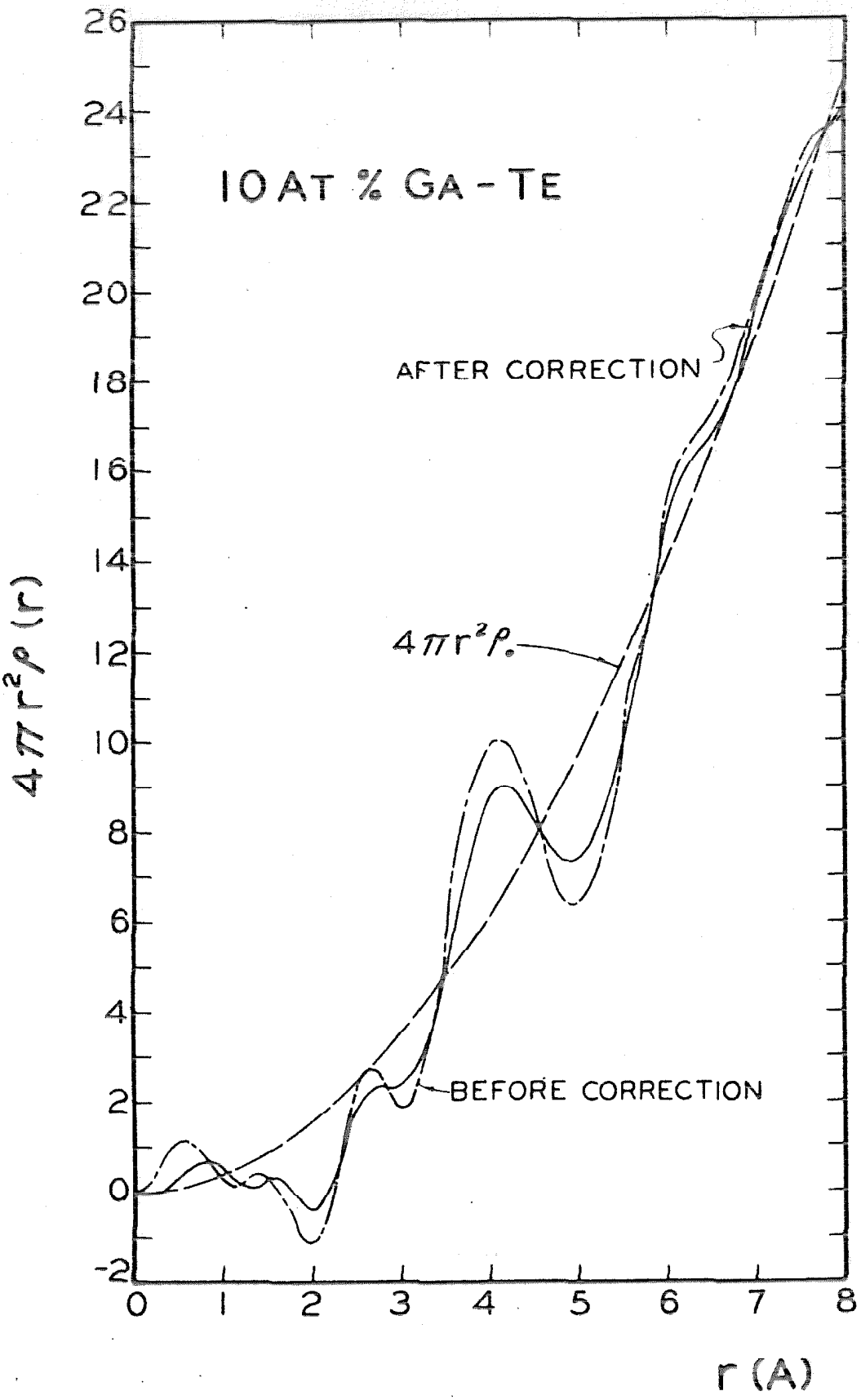

Fig. 7. Radial distribution curves for 10 at. % Ga; Te corresponding to corrected and uncorrected intensity data shown in Fig. 3.

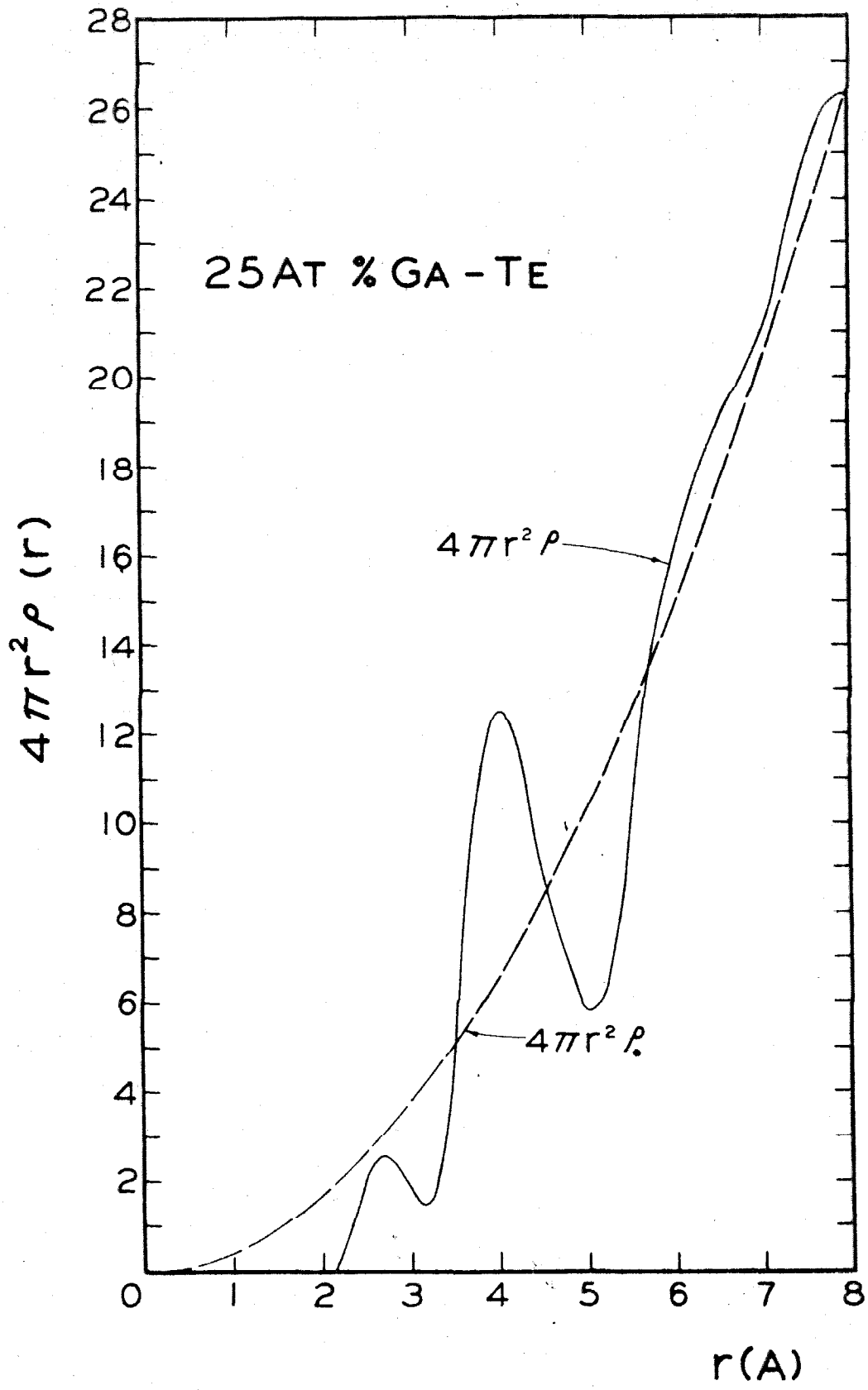

Fig. 8. Radial distribution curve for 25 at. % Ga;Te calculated from the intensity data shown in Fig. 4.

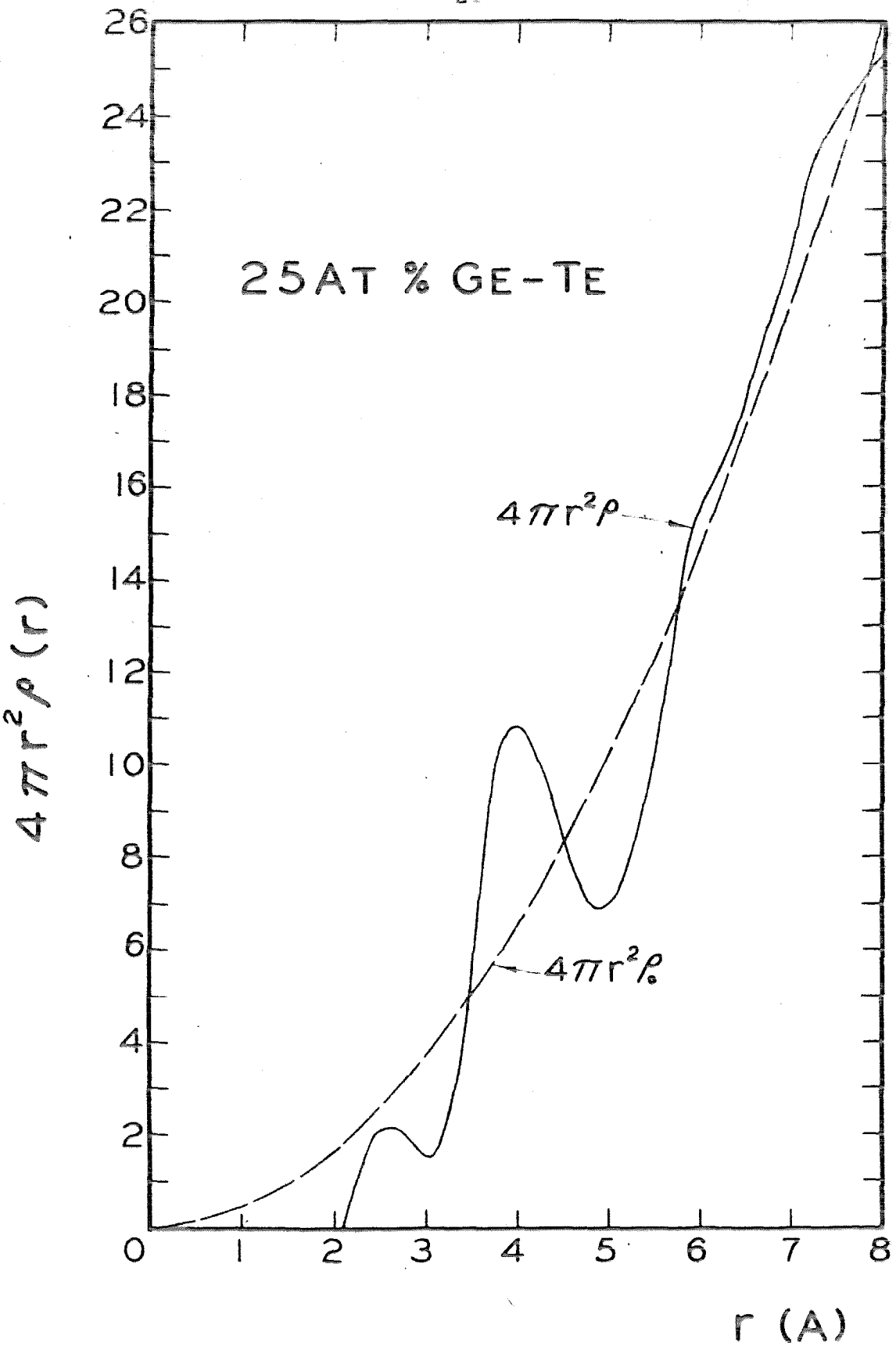

Fig. 9. Radial distribution curve for 25 at. % Ge; Te calculated from the intensity data shown in Fig. 5.

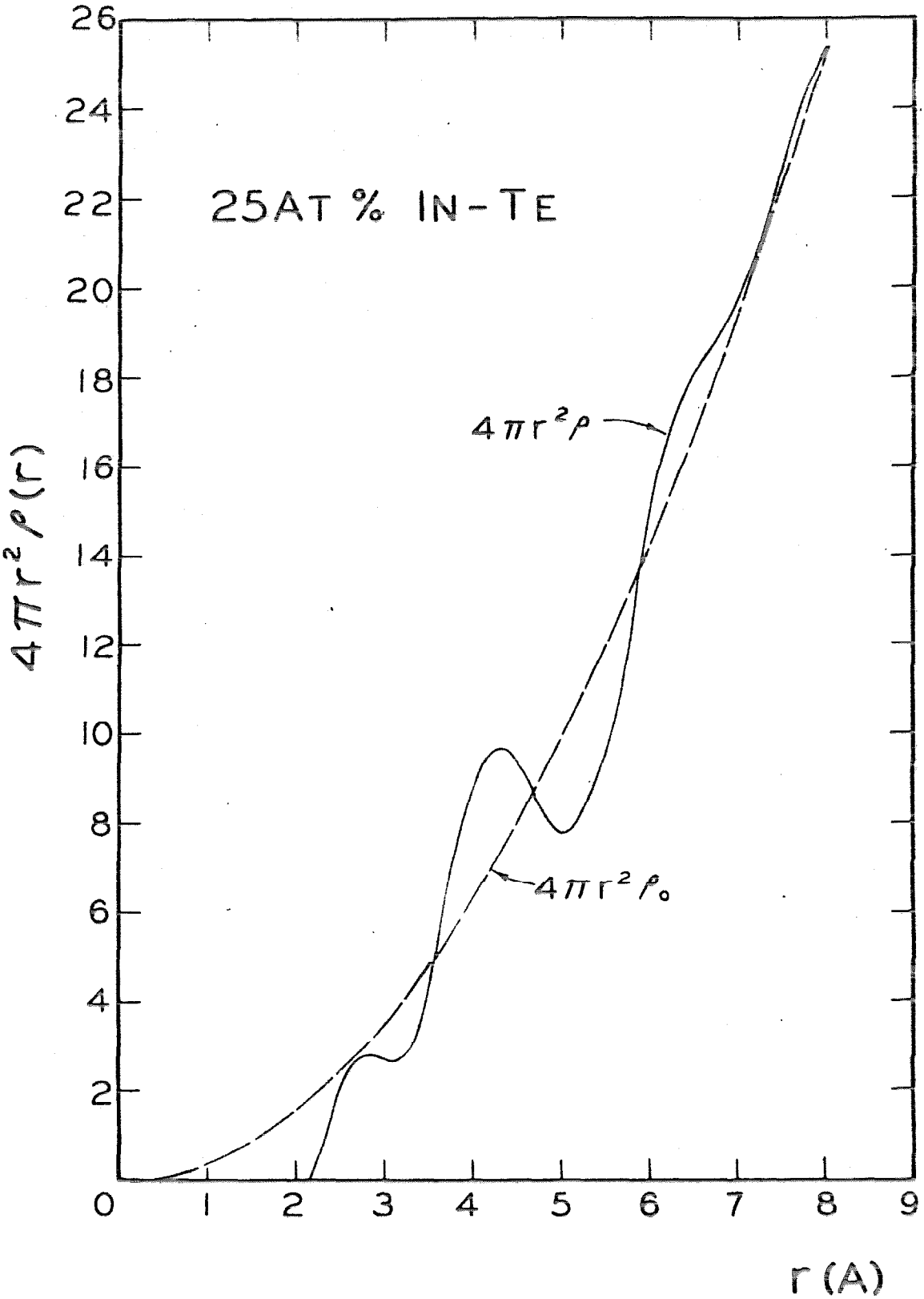

Fig. 10. Radial distribution curve for 25 at. % In;Te calculated from the intensity data shown in Fig. 6.

V. OTHER RESULTS AND DISCUSSION

As seen from Figs. 3-6, the intensity curves of different alloys show the same pattern with peaks at

$$\frac{\sin\theta}{\lambda} = 0.164 \pm 2,\quad 0.266 \pm 4,\quad 0.410 \pm 8\ \text{Å}^{-1}.$$

In fact, this observation is true throughout the ranges of the amorphous phase, i.e., 10 ~ 30 at.% Ga;Te, 10 ~ 25 at.% Ge;Te and 10 ~ 30 at.% In;Te. Consequently, the radial distribution functions for different alloys show very little difference (Table I).

In addition to the above mentioned alloys, amorphous phases of the same patterns were also observed in the quenched samples of certain other alloys. However, because of various difficulties in physical conditions, these alloys were not studied further.

1. In the range of 7 ~ 10 at.% Al;Te, only the amorphous phase was observed. However, because the compound Al_2Te_3 decomposes into H_2Te and Te readily while absorbing moisture, the range of the amorphous phase can not be extended.

2. At approximately 20 at.% Si;Te, the x-ray diffraction pattern showed the presence of the amorphous phase. The comparatively large loss in Te in the process of preparing and quenching alloys prevented controlling the alloy compositions.

3. In the range 15 ~ 35 at.% Cu;Te, the quenched alloys were partially amorphous. Up to 20 at.% Cu, lines that could be identified with hexagonal Te were observed; alloys of higher Cu content showed other unknown phases.

TABLE I. Interatomic distances and coordination numbers in amorphous phases

Alloy composition	First nearest neighbor		Second nearest neighbor	
	Distance (Å)	Coordination Number	Distance (Å)	Coordination Number
10 at. % Ga; Te	2.65	1.3	4.10	12.5
15 at. % Ga; Te	2.65	1.4	4.10	11.4
20 at. % Ga; Te	2.70	1.7	4.00	11.6
25 at. % Ga; Te	2.70	1.7	4.05	12.7
30 at. % Ga; Te	2.70	2.0	4.05	12.4
10 at. % In; Te	2.80	2.0	4.15	11.3
15 at. % In; Te	2.80	2.2	4.20	11.6
20 at. % In; Te	2.75	2.2	4.15	10.8
25 at. % In; Te	2.75	2.1	4.25	13.3
30 at. % In; Te	2.70	2.3	4.25	14.0
10 at. % Ge; Te	2.70	1.6	4.05	11.1
15 at. % Ge; Te	2.60	1.3	4.05	11.9
20 at. % Ge; Te	2.60	1.4	4.05	11.6
25 at. % Ge; Te	2.60	1.6	4.00	11.4

4. Around 10 at.% Sb;Te, the amorphous phase, weak but observable, coexisted with the strong hexagonal Te phase. Alloys of higher Sb content were quenched but they consisted of a mixture of crystalline and amorphous phases.

5. In alloys 20 ~ 40 at.% Tl;Te amorphous phases were observed. However, the results were not consistent possibly because the liquidus temperature is low (200 ~ 300 ^{o}C), and the quenching effect is easily annealed out at room temperature.

In the present work, it has been noticed that two different metastable phases appear in the as-quenched Te-base alloys. Besides the amorphous phases, simple cubic phases have been observed in the following alloys:

15 ~ 40 at.% Au;Te, 20 ~ 30 at.% Ag;Te, 10 ~ 20 at.% Bi;Te. Lattice parameters of these simple cubic phases are given in Table II.

Alloys around the compositions 14.5 at.% Pb;Te, 16 at.% Sn; Te, have also been tried by the same quenching technique. But for some unknown reason, the results were inconclusive as to which type of phase the detected phases belong.

The occurrence of either an amorphous or a single cubic structure in Te base alloys cannot be predicted at the present time. However, one trend can be observed. When elements of the same group in the periodic table are alloyed with tellurium, heavier elements with larger size of *atoms and more metallic in character favor the simple cubic structure.* According to this trend amorphous structures would exist in the quenched alloys 20 ~ 30 at.% As;Te. This system was not investigated because of the high arsenic vapor pressure from the molten alloy.

TABLE II. Lattice parameters of simple cubic phases

Composition	Lattice parameter (Å)
15.3 at.% Au;Te	3.073 ± 5
18.5 "	3.069 ± 2
19.2 "	3.071 ± 3
20.5 "	3.056 ± 2
23.0 "	3.045 ± 3
25.5 "	3.015 ± 4
28.0 "	3.005 ± 2
30.4 "	2.988 ± 2
33.8 "	2.967 ± 2
37.5 "	2.960 ± 2
40.4 "	2.945 ± 3
20.5 at.% Ag;Te	3.057 ± 2
23.0 "	3.054 ± 3
25.5 "	3.054 ± 3
28.0 "	3.053 ± 3
30.5 "	3.053 ± 3
10 at.% Bi;Te	3.18 ± 2
15 "	3.22 ± 3
20 "	3.26 ± 5

The equilibrium crystal structures of tellurium and selenium are isomorphic and consist of spiral chains. Each chain has three atoms per turn and all chains lie parallel to one another to form hexagonal nets in a crystal. The relation between this hexagonal chain and the simple cubic structures has been noticed by von Hippel (42), and has been calculated in a previous report (43). The hexagonal lattice of Te can be viewed as a slightly distorted simple cubic lattice with three nearly orthogonal planes ($89^{o}37'$, $96^{o}15'$, $96^{o}15'$) which interact 0.430 Å from a given Te atom. Of the six nearest neighboring atoms, two are at 3.154 Å and four at 3.444 Å from the point of intersection. The possibility of obtaining the amorphous phase has also been connected with the formation of long chain molecules (24). Selenium has been obtained metastably in the amorphous as well as the simple cubic forms (44). Although pure tellurium is known only to exist in the chain-hexagonal lattice, by alloying with proper amounts of a second element, the results obtained here indicate that the three types of structures mentioned above are truly related.

Attempts were made to measure the electrical resistivity of the quenched alloys. This was done by pouring Thalco boat resin into a Teflon mold placed over a specimen quenched on copper and allowing the resin to set for 12 hrs (28); rather coherent foils can be obtained as cast onto the face of the insulating plastic block. With an ohmmeter, resistivities of the quenched foils of different alloys are crudely estimated. The results thus obtained can be only regarded as qualitative. Nevertheless, it can be concluded that in all cases the resistivities of the amorphous phases are 3 to 5 orders of magnitude higher than those of the simple cubic phases. In other words, the bonding in the latter

phases is more metallic in nature.

On fusion, the resistivity of selenium increases abruptly. The magnitude of the increase depends strongly on the thermal history of the selenium sample and is relatively small (2 ~ 3 times) for a sample of high purity (45). On the other hand, the transition of selenium from the amorphous state to the liquid is not accompanied by any noticeable change of electrical conductivity (46). This is considered to be in full agreement with the absence of a structural change (21, 22).

In contrast, the resistivity of tellurium decreases sharply from 6×10^{-3} to 5×10^{-4} ohm-cm upon melting (47). Other electrical properties of tellurium such as the Hall coefficient and the thermoelectrical power (47) also change discontinuously near the melting point. Lark-Horovitz and his students have interpreted these abrupt changes as due to the destruction of order among tellurium atom-chains in the process of melting while each chain remains relatively intact.

Table III shows the interatomic relations in a crystalline tellurium lattice and within the structure of tellurium-rich amorphous alloys as well as in the liquid tellurium structure at 465 ^{o}C (27). In making a comparison, it may be visualized that the amorphous structure is still composed of atom-chains which are shrunken and fail to align themselves into the crystalline structure. The fact that both the bond distance and the number of nearest neighbors are preserved indicates that the covalent bonding of atoms is still dominant in the amorphous structure.

TABLE III. Comparison of structures of crystalline tellurium, tellurium-base amorphous alloys, and liquid tellurium.

Crystalline tellurium				Amorphous alloys			Liquid tellurium (465 °C)		
Nearest Neighbor	Interatomic distances (Å)	No. of atoms	Location	Peaks	Interatomic distances (Å)	No. of atoms	Peaks	Interatomic distances (Å)	No. of atoms
1st	2.864	2	same chain	1st	2.65-2.75	1.6	1st	2.93	2.3
2nd	3.468	4	adjacent chain	2nd	4.05-4.20	12.0-12.5	2nd	4.4	--
3rd	4.457	6	adjacent chain						
4th	4.463	2	same chain						

VI. THE FORMATION OF AMORPHOUS PHASES

Congener elements selenium and tellurium have the same equilibrium crystalline structure but show remarkably different behaviors when undercooled from their liquid states. As has been mentioned in Sec. I, pure selenium can be obtained in the amorphous form by several distinct methods and the literature is still in confusion as to whether or not the amorphous form of pure tellurium can be obtained by undercooling (48). In fact, pure tellurium subjected to the extremely fast cooling technique used in this investigation has been always crystalline. Since variations in the atomic configuration from the liquid state to the crystalline state always involves a process of diffusion, and approximately similar adjustments must occur during viscous flow, it is thus to be expected that the viscosity suffices as an indicator of this transition. The viscosity data of pure tellurium and selenium shown in Fig. 11 (49-51) reveal a noticeable distinction between these two elements near their melting points. This distinction may be considered as an evidence that selenium can be readily chilled into amorphous form and tellurium can not. The viscosity-temperature curve of selenium is typical for a simple glass-forming material whose viscosity lies between 0.01 and 10 poise at temperatures between its normal melting and boiling points, and increases rapidly and continuously with decreasing temperatures. But for tellurium the temperature-viscosity relation shows hysteresis character. Along the cooling curve, the viscosity remains low even when sufficiently undercooled; hence, tellurium atoms are still mobile enough to crystallize upon further cooling. The heating branch

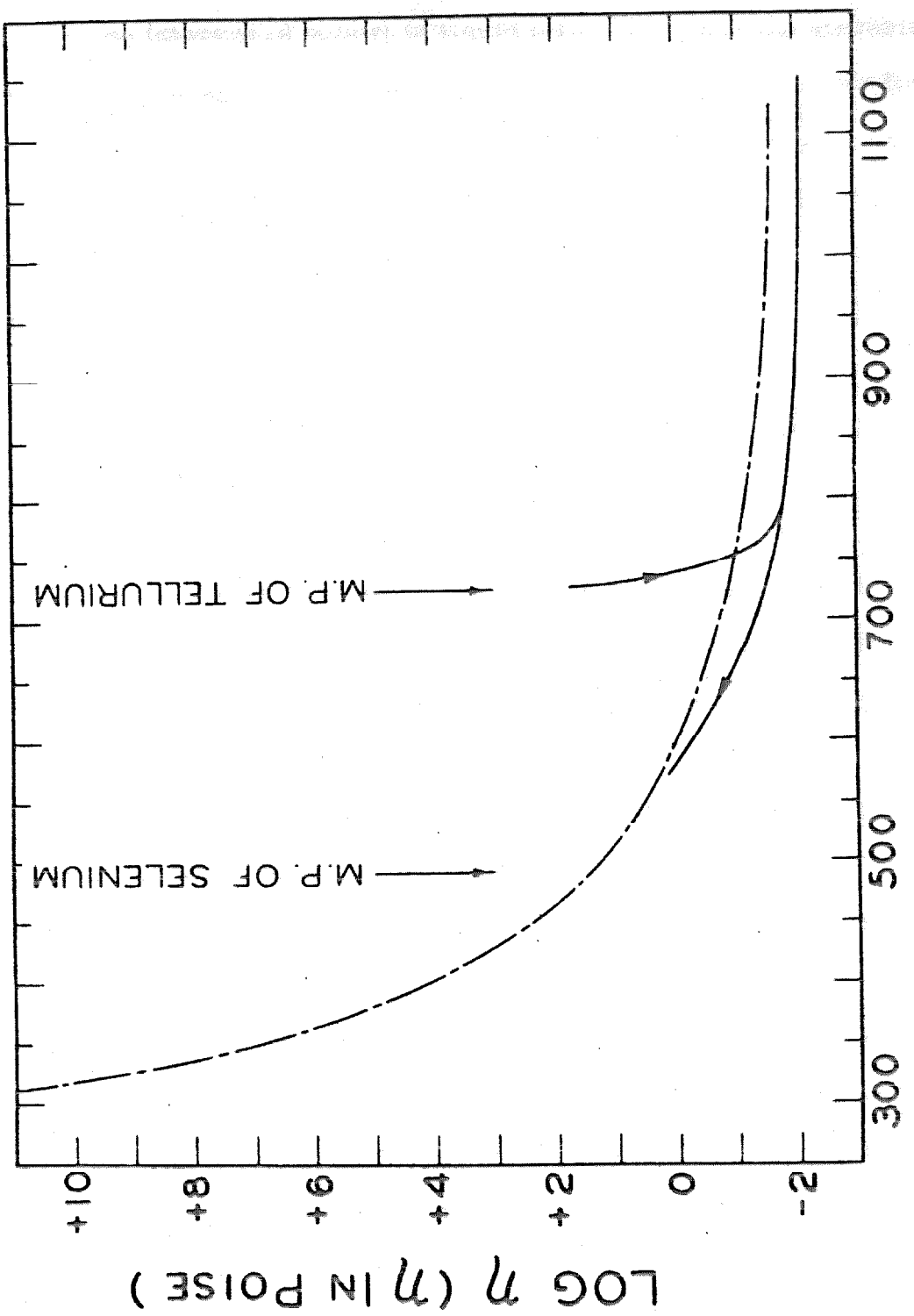

Fig. 11. Viscosity curves for pure tellurium and pure selenium.

of the curve may also be correlated with the gradual covalent-metallic transition (discussed below) in liquid tellurium since the viscosity of metallic-binding liquid is often lower than that of covalent-binding liquid. The viscosity approach to the problem of amorphous phases in tellurium alloys obtained in the present investigation is difficult since no viscosity data of these alloys exists. Thus a systematic study of viscosity-temperature relationship of such systems may be of great interest.

Since the liquid-solid transition is mainly controlled by diffusion and hence is temperature dependent, the fact that tellurium-base amorphous alloys can be obtained in this investigation can be simply explained as due to the lowering of liquidus temperatures. This is in accord with the theory proposed by Turnbull and Cohen (52, 53) that the addition of impurities depresses the melting temperatures and enhances the glass-forming tendency. Considering the phase diagrams in Figs. 12-14, the compositions of the amorphous alloys are indeed in the vicinities of corresponding eutectic points (54, 55).

Usually glasses or other amorphous materials composed of two or more components cover a range of composition because of the fact that they are mixtures or solutions rather than exact chemical compounds. It is essential for glass-forming that these components be highly inter-soluble in the liquid state in this range of composition. It has also been noticed that when a range of composition where glass-formation is observed includes a eutectic point or other changes in liquidus temperature, the amorphous phases of different compositions are not of the same

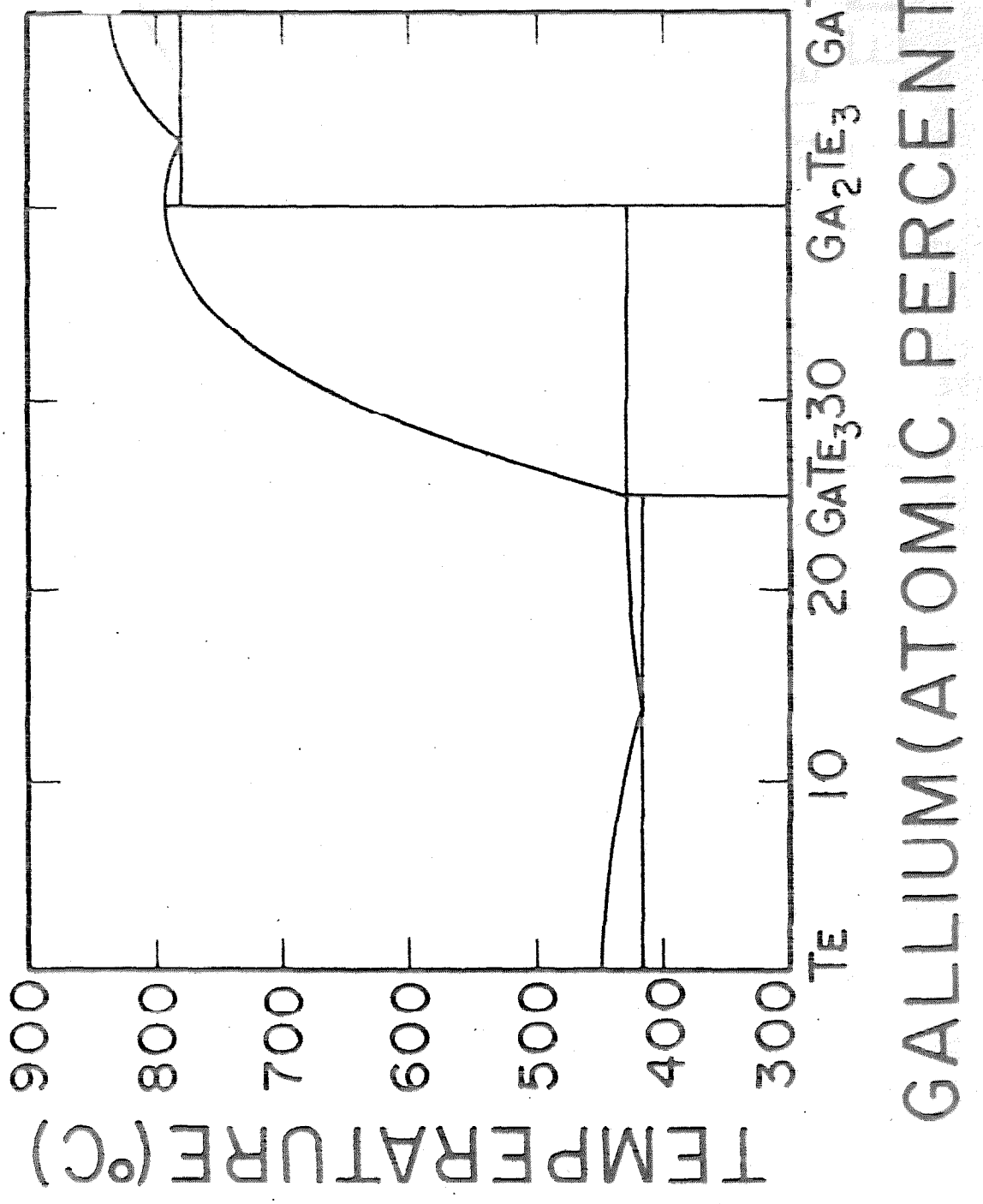

Fig. 12. Tellurium-rich side of equilibrium phase diagram of Te-Ga system

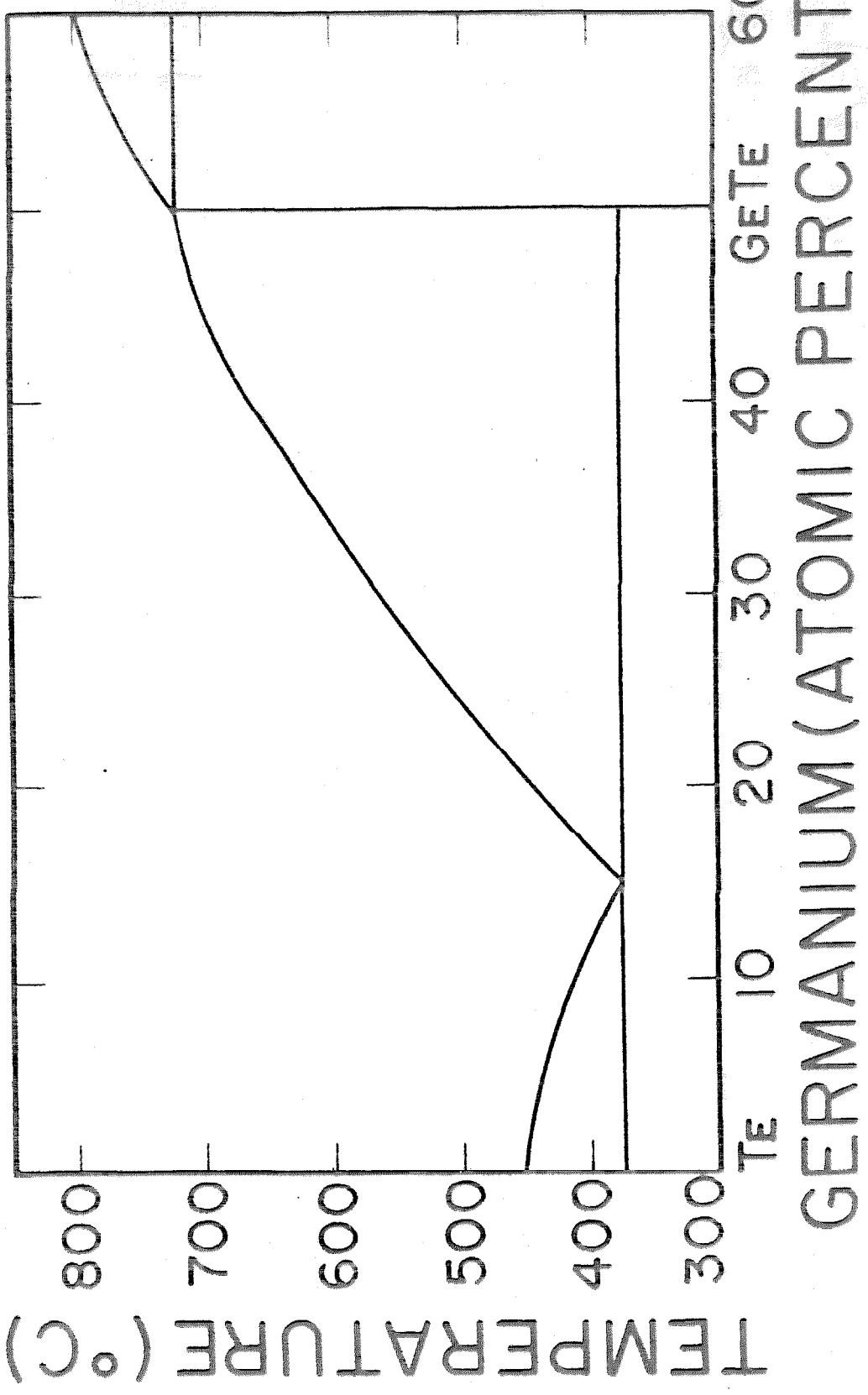

Fig. 13. Tellurium-rich side of equilibrium phase diagram of Te-Ge system

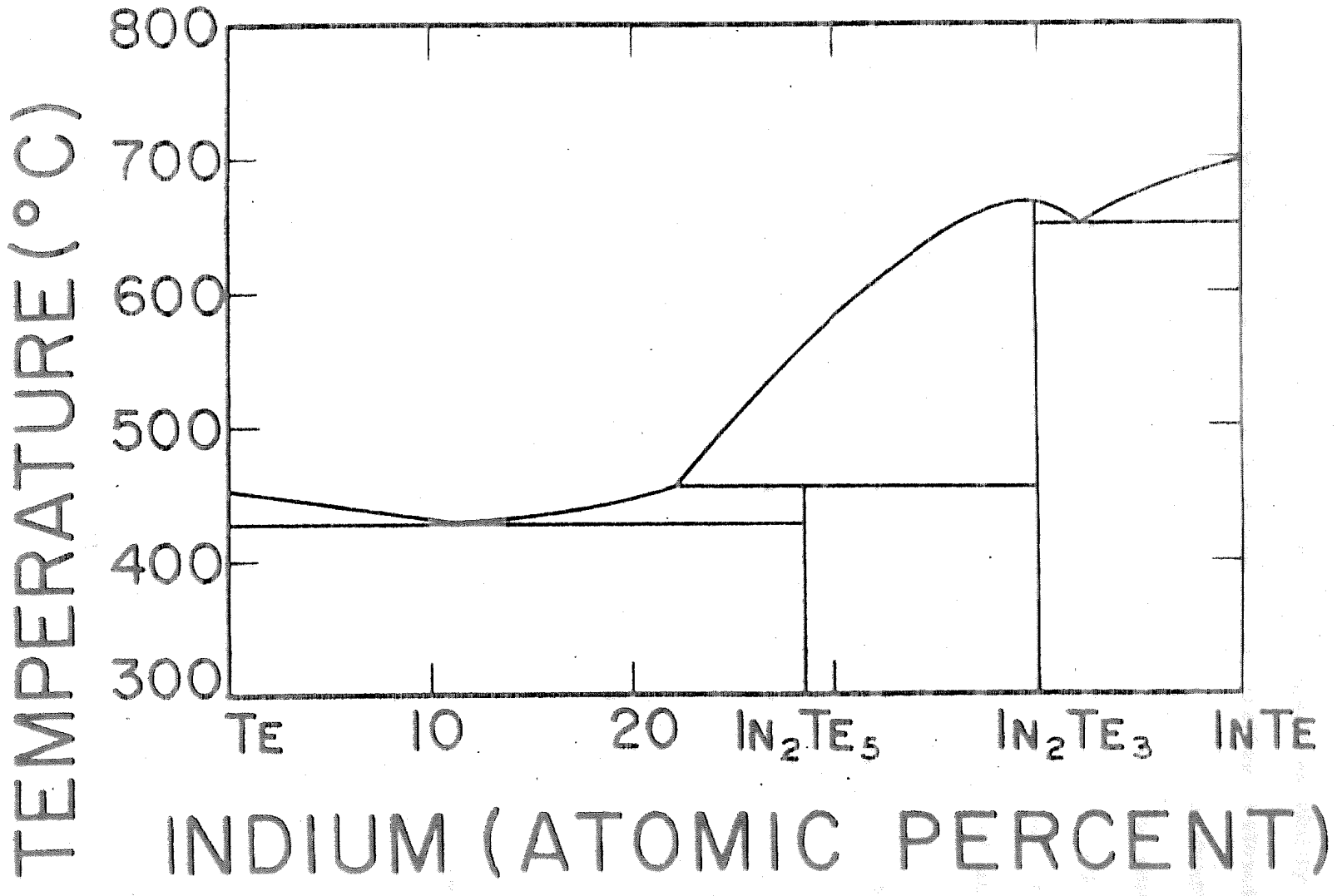

Fig. 14. Tellurium-rich side of equilibrium phase diagram of Te-In system.

stability. Since the liquidus curves indicate the change in solubility of the primary phase in the melt with change in temperature, below the liquidus the melt becomes supersaturated with respect to the primary phase and crystallization can take place. Consequently, with the same cooling rate, the steeper the liquidus curve, the greater the amount of supersaturation and the greater the probability of crystallization. Thus it is conceivable that the most stable amorphous phase is to be obtained at the composition where the liquidus is of lesser slope. Hamilton and Cleek have observed that this is true for many systems of glasses (56). However, possibly because the eutectic points are located too close to the tellurium side and hence the crystallization of tellurium lattice can not be suppressed, this observation can not be proved in the result of the present investigation.

In recent years the idea of chemical bonds as associated with glass-formation has been put forward. In the process of glass-forming, covalent binding is considered to be essential. An intuitive reason for such consideration is that the ionic binding with electrostatic Coulomb fields and the metallic binding, with conduction electrons spread uniformly and symmetrically in all directions, are long-range in character, whereas the covalent binding is directional, localized and hence has only a short-range influence. Winter (57) has proposed an empirical condition of vitrification that for glass formation the average number of p-electrons per atom in the substance involved has to be in the range from 2 to 4. This simple condition covers many glass-forming materials such as SiO_2 (3.33), B_2O_3 (2.80), BeF_2 (3.33), Se and S (4.00) etc. surprisingly well although there are many exceptions yet to be explained. In particular,

the present results 10 ~ 30 at.% Ga;Te, 10 ~ 30 at.% In;Te, (3.1 ~ 3.7) and 10 ~ 25 at.% Ge;Te (3.5 ~ 3.8) seem also to follow this condition. Since it is hard to believe that p-electrons control the process of glass formation, the experimental fact of glass-forming materials all having 2 to 4 p-electrons per atom can only be taken as indicating the specific structures with low coordination number and covalent binding. Thus a natural question to ask is why many other semiconducting materials, in which the binding is covalent, do not vitrify?

Since the mechanism of vitrification is due to the undercooling of melts, it is clear that in the consideration of glass-forming capacity of any material it is appropriate to examine the material in its liquid state as well as in its solid state. In the study of electrical conductivity of semiconductors, it has been found that semiconducting materials which fail to transform into glassy state such as silicon, germanium, the antimonides of gallium and indium, lead selenide and telluride, and bismuth selenide and telluride, all become metallic after melting (58-63). In liquid cadmium and zinc tellurides, and in zinc selenide which also fail to vitrify, the conduction is not metallic but is believed to be ionic. On the other hand, the semi-conducting properties of selenium which is very easy to vitrify persist into the fused state up to 310 ^{o}C with no indication of a change to metallic conduction (27). This correlation between the glass-forming possibility and the metallic-covalent transition of chemical bonds has been held strongly by the Russian author Kolomiets and his school (64), and their study on the conductivity of melts of the pseudobinary system As_2Se_3-As_2Te_3 is also in support of this observation (65, 66). With pure tellurium, the case appears to be borderline.

Tellurium remains semiconducting immediately after melting but gradually changes into metallic state as the temperature increases. It has been estimated that the atomic binding in liquid tellurium at 610 °C is 40% metallic (27, 67) and it is generally believed that tellurium will become entirely metallic when the temperature is raised higher. Thus in an undercooled melt, the metallic binding may persist in tellurium and hence tellurium is prevented from vitrification. (This is consistent with the viscosity data.) It might be tentatively concluded that a necessary condition for semiconducting materials to transform into glassy state is the existence of covalent binding in the material both in the solid and in the liquid states. Thus it appears pertinent to study systematically the electrical conductivity of other semiconductors in connection with their solid-liquid transition.

In conclusion, it is considered that pure tellurium with its chain-structure is potentially capable of vitrification. By alloying with a minor part of another element, the binding of tellurium becomes either more covalent or has a tendency to become metallic. The two types of structures found in the present investigation may be a result of these two different effects introduced by a second element. The amorphous structure and the liquid structure at its semiconducting stage are essentially the same. Since the hexagonal chain structure of tellurium is closely related to a simple cubic lattice and the metastable phases obtained by quenching has retained some of the characteristics of the liquid state, it may be even speculated that the liquid structure of tellurium at high enough temperature (where metallic conduction is expected) might be compatible with a simple cubic lattice extended to a few atomic distances.

REFERENCES

1. P. Debye and P. Scherrer, Göttingen Nachrichten 16 (1916).

2. W. H. Keesom and J. de Smedt, Proc. Amst. Akad. Sci., 25, 118-24 (1922); 26, 112-115 (1923).

3. N. S. Gingrich, Rev. Mod. Phys. 15, 90-110 (1943).

4. K. Furukawa, Repts. Prog. Phys., Phys. Soc. (London) 25, 395-440 (1962).

5. R. F. Kruh, Chem. Rev., 62, 319-346 (1962).

6. F. Zernike and J. A. Prins, Z. Phys., 41, 184-194 (1927).

7. P. Debye and H. Menke, Phys. Z., 31, 797-798 (1930); Ergeb. Techn. Rontgenk., 2, 1 (1931).

8. C. Finbak, Acta Chem. Scand., 3, 1279-1292 (1949); 3, 1293-1348 (1949).

9. O. Burgen and C. Finbak, Acta Chem. Scand., 8, 829-834 (1954).

10. O. Bastiansen and C. Finbak, Arch. Math. Naturvidenskab., 47, 153-163 (1947).

11. B. E. Warren, J. Appl. Phys., 8, 645-654 (1937).

12. H. Richter, Z. Naturf., 13A, 32-36 (1958); Fortsch. Physik, 8, 493-527 (1960).

13. H. Richter and S. Steeb, Z. Metallk., 50, 369-378 (1959).

14. S. Urnes, Modern Aspects of the Vitreous State (1960), I, 10-37.

15. Bibliography on Glass Structure, Glass Industry, 41 (1960), 396-397, 440-443, 492-495, 557-560, 630-633, 696-697; 42 (1962), 29-30, 84-85, 136-139, 201, 254-257, 390-391, 449-451, 511-513.

16. H. Richter and G. Breitling, Arbeistag. Festkorperphysik, 2, 207-219 (1954).

17. K. Das Gupta and B. B. Ray, Indian J. Phys., 15, 389-399 (1941).

18. A. K. Graham, H. L. Pinkerton and H. J. Boyd, Electrochem. Soc. J., 106, 651-654 (1959).

19. H. Richter, W. Kulcke and H. Specht, Z. Naturforsch., 7a, 511-532 (1952).

20. E. Kipphan, German Patent 834,095 (March 17, 1952).

21. H. Richter and F. Herre, Z. Naturforsch., 13a, 874-885 (1958); Naturwissenschaften, 44, 31 (1957).

22. G. Frohnmeyer, H. Richter, and G. Schmelzer, Z. Metallk., 46, 689-692 (1953).

23. H. Grimminger and H. Richter, Naturwissenschaften, 42, 256 (1955).

24. A. Winter, J. Am. Cer. Soc., 40, 54-58 (1957); 41, 464-466 (1958)

25. G. W. Morey, Properties of Glasses, (1958).

26. J. M. Stevels, Handbuch der Physik, 13, 510-644 (1962).

27. R. C. Buschert, Ph.D. Thesis, Purdue University (1957).

28. W. Klement, Jr., Ph.D. Thesis, California Institute of Technology, (1962).

29. P. Duwez and R. H. Willens, Trans. Met. Soc., AIME, 227, 362-365 (1963).

30. B. D. Cullity, Elements of X-ray Diffraction, (1956).

31. A. Guinier, X-ray Diffraction, (1963).

32. A. Claassen, Phil. Mag., 9, 57-65 (1930).

33. A. Rusterholz, Helv. Phys. Acta, 4, 68-121 (1931).

34. A. J. Bradley, Proc. Phys. Soc. (London), 47, 879-899 (1935).

35. W. Heisenberg, Phys. Z., 32, 737-740 (1931).

36. L. Bewilogna, Phys. Z., 32, 740-744 (1931).

37. R. W. James, The Optical Principles of the Diffraction of X-rays, (1958).

38. H. H. Paalman and C. J. Pings, Rev. Mod. Phys., 35, 389-399 (1963).

39. J. Krogh-Moe, Acta Cryst., 9, 951-953 (1956).

40. P. Debye, Ann. Phys., 46, 809-823 (1915).

41. H. P. Klug and L. E. Alexander, X-ray Diffraction Procedures for Poly-crystalline and Amorphous Materials, (1954).

42. A. von Hippel, J. Chem. Phys., 16, 372-380 (1948).

43. H. L. Luo and W. Klement, J. Chem. Phys., 36, 1870-1874 (1962).

44. A. I. Andrievskii, I. D. Nabitovich, and P. I. Kripyakevich, Soviet Phys. Doklady, 4, 16-19 (1959).

45. F. Eckhart, Ann. Phys., 14, 233-252 (1954).

46. A. F. Ioffe and A. R. Regel, Prog. in Semiconductors, 4, 237-291, (1960).

47. A. Epstein, H. Fritzsche and K. Lark-Horovitz, Phys. Rev., 107, 412-419 (1957).

48. C. G. Oancha, J. Teodorescu and P. Cristya, Soviet Phys. - Crystallography, 7, 451-453 (1963).

49. A. I. Blum and A. R. Regel, J. Tech. Phys. Moscow, 23, 964-975, (1953).

50. A. Eirsenberg and A. V. Tobolsky, J. Polymer Sci., 46, 19-28, (1960); 61, 483-495 (1962).

51. K. Uberreiter and H. J. Orthman, Kolloid Z., 123, 84-91 (1951).

52. D. Turnbull and M. H. Cohen, Modern Aspects of the Vitrous State, (1960), 1, 38; J. Chem. Phys., 34, 120-125 (1961).

53. M. H. Cohen and D. Turnbull, Nature, 189, 131-132 (1961).

54. M. Hansen and K. Anderko, Constitution of Binary Alloys, (1958).

55. P. C. Newman, J. C. Brice and H. C. Wright, Philips Res. Repts., 16, 41-50 (1961).

56. E. H. Hamilton and G. W. Cleek, J. Research Natl. Bur. Standards, 60, 593-596 (1958).

57. A. Winter, Compt. rend., 240, 1, 73-75 (1955); 240, 19, 1878-1880 (1955).

58. A. I. Blum, N. P. Mokrovskii and A. R. Regel, Bull. Acad. Sci., USSR, 16, 139-153 (1952).

59. R. W. Keyes, Phys. Rev., 84, 367-368 (1951).

60. A. Epstein, Ph. D. Thesis, Purdue University (1954).

61. N. P. Mokrovskii and A. R. Regel, J. Tech. Phys., Moskow, 22, 1281-1289 (1952); 23, 779-782 (1953).

62. G. Busch and O. Vogt, Helv. Phys. Acta, 27, 241-248 (1954).

63. A. R. Regel, Doctorate Dissertation, Leningradskii Gos. Universitet in A. A. Zhdanova (1957).

64. N. A. Goriunova and B. T. Kolomiets, Soviet Phys.-Tech. Phys., 3, 1766-1775 (1958); The Structure of Glass - Proceedings of the Third All-Union Conference on the Glass State, Leningrad, 1959 (1960), 2, 58-63.

65. T. N. Vengel and B. T. Kolomiets, Soviet Phys.-Tech Phys., 2, 2314-2319 (1957).

66. B. T. Kolomiets and V. P. Pozdnev, Soviet Phys.-Solid State, 2, 23-29 (1960).

67. V. A. Johnson, Phys. Rev., 98, 1567 (1955).